Vibronic theory of the stability and hysteresis in bistable mixed-valence molecular salts

K. Boukheddaden and F. Varret
Laboratoire de Magnétisme et Optique, CNRS, Université de Versailles Saint-Quentin,
45 Avenue des États Unis, 78035 Versailles cedex, France
(Received 27 December 1994; revised manuscript received 22 November 1995)

We previously proposed a two-orbital cooperative adaptation of the vibronic Piepho-Krausz-Schatz model, for modeling the solid-state properties of biferrocenium mixed-valence salts. The resulting molecular ferroelectric model, treated in mean-field approach, leads to remarkable double-reetrance at low temperature, following the sequence ferro-para-ferro-para-electric with increasing temperatures. Here we investigate some aspects of the phase diagram of the system: we unambiguously assess the metastable character of the second-reentrant state and we study the hysteresis loops associated with the first-order transitions which result from orbital crossovers in the model. [S0163-1829(96)03918-5]

I. INTRODUCTION

Bistable molecular systems[1–3] are fascinating because they offer original potentialities for information storage[4] at the molecular level. Molecular bistability requires a thermal equilibrium (or quasiequilibrium) between two molecular states exhibiting physical properties (for example optical absorption, spin state ...) different enough to provide a clear-cut characterization. Molecular bistability can be associated with an electron transfer somewhere in the molecule, in case of electronic or vibronic lability.[5]

The most studied examples of bistable systems are linked with spin conversion,[6–8] resulting from an intraionic transfer triggered by temperature, pressure, light, or ligand photo-isomerization.[9,10] Here we deal with materials involving an intramolecular electronic transfer: mixed-valence molecular complexes (see Refs. 11, 12 for basic properties), and we describe their possible molecular bistability.

Most of observations relevant to molecular bistability have been obtained in the solid state, in presence of intermolecular interactions leading to cooperative phenomena: for example the low-temperature electron trapping in biferrocenium mixed-valence salts (Refs. 13 and 14). The mixed-valence molecular solid actually forms a coupled bistable network exhibiting an order disorder phase transition which may be ferro-paraelectric (it is worth nothing, for comparison, that spin transitions are not order disorder). The mixed-valence network can be modeled, in the Born-Oppenheimer approach, through discrete approximations: the Ising model ($S=1/2$) (Refs. 15 and 16) or the Blume-Emery-Griffiths [BEG, $S=1$ (Ref. 17)] Hamiltonian.[18] Here we treat the vibronic Hamiltonian of the mixed-valence network, *beyond* the adiabatic approximation, thus following the dynamic approach proposed by Piepho, Krausz, and Schatz (PKS) for the isolated molecule.[19,20] We first adapted the PKS model to the biferrocenium molecule[21] and then developed a cooperative PKS model,[22,23] which is able to reproduce the second-order localized-delocalized transitions of some biferrocenium derivatives.

However, the biferrocenium cation possesses a quasidegenerate highest occupied molecular orbital (HOMO) involving two orbitals with extremely different properties: a ''good localizer'' (d_{xy}) and a ''bad localizer'' ($d_{x^2-y^2}$), with transfer integrals in the ratio 1:50.[21] Such a pecularity led us to investigate a *two-orbital* cooperative PKS model.[24,25] In the two-orbital model, the thermodynamic competition occuring between vibronic states based on the good and bad localizer orbitals, led to predictions of a remarkable variety of behaviors: second- and first-order para-ferroelectric transitions, double reentrance, and double transitions. The two-orbital model enabled us to reproduce the first-order transition displayed by biferrocenium tri-iodide.

The double reentrance which consists of a ferro-para-ferro-paraelectric sequence on increasing temperature, has been previously predicted by other models: (i) the ferroelectric dipolar model of Tsukerblatt and co-workers,[26,27] (ii) the BEG model using Monte Carlo Metropolis algorithm,[28] and (iii) the Bethe and the cluster-variational method.[29] But so far the stability of the second-reentrant phase has not been determined. The first aim of the present work is to examine this reentrant phase using our cooperative two-orbital vibronic model.

The second aim is to determine the hysteresis loops associated with the first-order transitions; we also systematically identify the stable and unstable character of the coexisting phases, in the scope of future application to information storage. The present report is organized as follows: Section I contains the physical grounds of the model; Section II provides the vibronic model and computations; Section III contains the results and discussion. In the Appendix the vibronic matrix elements and four-level discrete model are shown.

II. THE PHYSICAL BASIS OF THE MODEL

Structural data[30,31] concerning molecular salts containing symmetrical mixed-valence units show that electron trapping is associated with an asymmetric distortion of the molecular unit, the so called ''breathing-mode,'' Q_-, which is the out-of-phase combination of the symmetrical stretching modes of the moieties, (the in-phase combination Q_+ which is not involved in the one-orbital PKS model,[19] will be referred to in the further discussion). The experimental observation of a breathing distortion provided evidence for a vibronic coupling between the electronic states (A^*B and AB^*, accord-

ing to the moiety the electron is trapped in) and the molecular distortion as suggested by Hush.[12]

In the PKS model, the energies of A^*B, AB^* states are shifted by $\pm\lambda Q_-$, where λ is the vibronic coupling parameter; the electron transfer between A and B is ensured by a transfer integral J, which is the tunneling matrix element between A^*B and AB^*; the stability of the system is provided by the elastic energy of an harmonic oscillator, the frequency of which is that of the stretching mode of uncoupled moities, i.e., that of the breathing mode.

These three ingredients (vibronic energy, elastic energy, transfer integral) lead to all possible behaviors of the isolated mixed-valence unit. This is easily visualized using static configurational diagrams (adiabatic energies versus distortion parameter Q_- such as in Fig. 1), in the shape of a single or double well, respectively, corresponding to delocalized or localized states.

The dynamic, nonadiabatic approach provides the value of the transfer rate between the two wells (i.e., the electron transfer rate), which is essential for understanding the experimental data according to the measuring frequencies. Computed data for the biferrocenium cation can be found in Ref. 21. They show, in agreement with the *Mössbauer* data on diethyl biferrocenium triiodide,[22,23] that the transfer rates are rather high ($>10^8$ s^{-1}). We consider here the case where all relaxation rates between vibronic states, are high with respect to the experimental measuring times, and accordingly we calculate all quantities in terms of thermal average values. In this dynamic view, the electron trapping exclusively results from an asymmetric potential, which disymmetrizes the configurational diagram, and merely corresponds to the energy difference $E(AB^*)-E(A^*B)=2W_d$.

In the solid state, such asymmetric potentials are due to the dipolar electric fields created by electron trapping in the neighboring units; in a first approach, they depend linearly on the distortion of these neighboring units. We thus introduced cooperativity, in a mean-field approach, through the self-consistent asymmetric potential:

$$W_d=\eta\langle Q_-\rangle,$$

where η is the intermolecular coupling parameter and $\langle Q_-\rangle$ the order parameter of the problem.

Here it is worth mentioning that the existence of a nonzero transfer integral can inhibit, at zero temperature, the onset of dipolar ordering: a ''quantum paraelectric phase''[32,33] (such as predicted by the transverse Ising model[34,35]) is deduced for small values of the cooperativity parameter.[36]

The second point to be considered is the quasidegeneracy of the HOMO of the moieties. The ''two-orbital model'' involves four electronic states instead of two in the previous one-orbital PKS model. We show in Fig. 1(b) a schematic configurational diagram adapted to the case of the biferrocenium cation, based on the coexistence of a double-well and a single-well orbital, uncoupled to each other because of molecular symmetry (a common mirror plane for both moieties). The localizing properties of the two orbitals are easily differentiated by applying an external potential [Fig. 1(c)]: the single (double) well is a bad (good) localizer.

The thermodynamic competition between the two orbitals (actually between vibronic states based on the two orbitals)

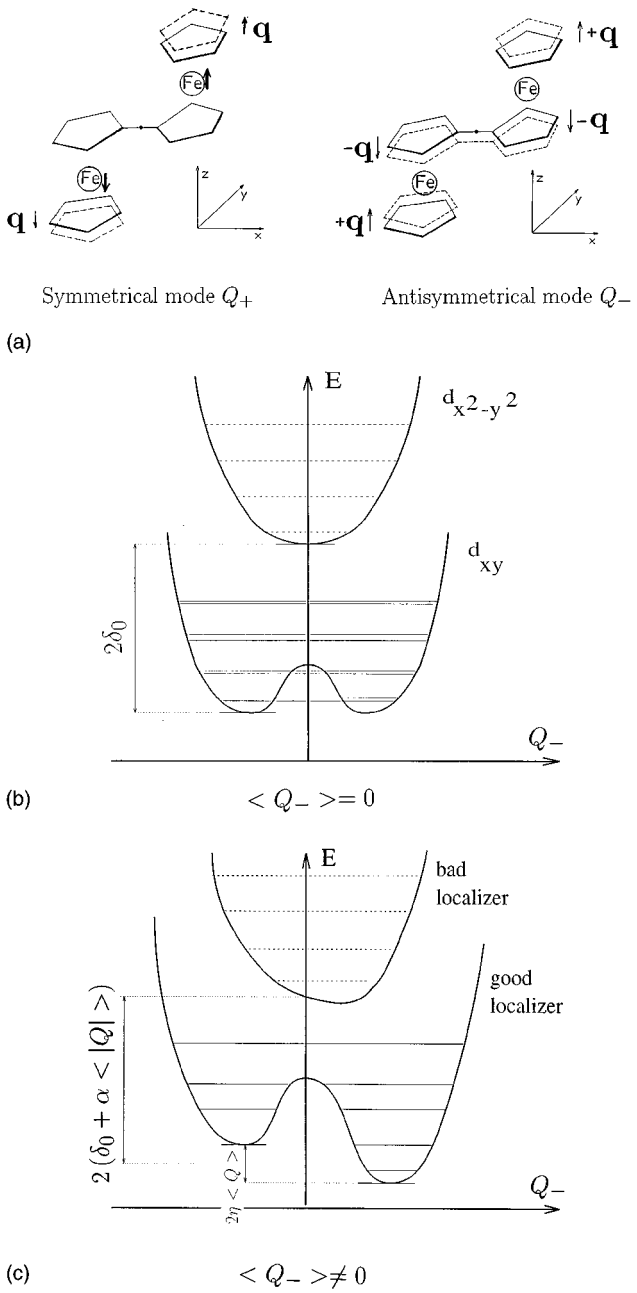

FIG. 1. (a) Distortion modes Q_+, Q_- of the biferrocenium cation; (b) Simplified configurational diagrams restricted to the lowest state of each orbital; horizontal lines depict the vibronic states; δ_0 is the ligand-field parameter; (c) Effect of an assymmetric potential. Molecule in the ferroelectric state (ordered).

is the cornerstone of the present work. It is mainly governed by the energy gap between the two orbitals of the isolated moiety: $\delta=E(d_{xy})-E(d_{x^2-y^2})$, written here for ferrocene moieties; δ is a low-symmetry ligand-field term, mainly depending on the substituents on the moieties, but also on the counter anions and on packing of the system in the solid state.

The double reentrance phenomenon can be obtained with a constant value of the ligand field (in a narrow range of value, see Sec. IV A). The effect of the thermodynamic competition is easily illustrated in the following case, corresponding to curve (4) in Fig. 2: the ground vibronic state is a

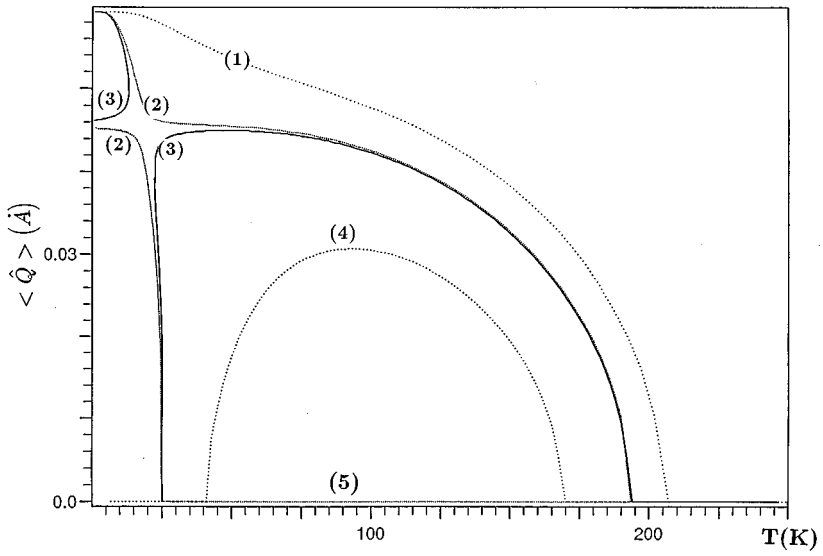

FIG. 2. Thermal dependence of the order parameter for several values of the ligand-field parameter δ_0, labeled from 1 to 5 according to sections (I)–(V) of the text (in Sec. IV A).

bad localizer; the cooperativity parameter is small enough to result in a low-temperature quantum paraelectric phase; low-lying good-localizer excited states can be populated at moderate temperature. This results in an ordered phase between two critical temperatures; the low-temperature phase is ''reentrant.'' The ordering of the system is due to the excited states, similarly to magnetic systems with a singlet ground state.

On the other hand, the first-order transitions are due to orbital crossovers resulting from a thermodynamic competition speeded up by a temperature-dependent ligand field of adequate sign. The latter can originate from a cooperative distortion, according to a totally symmetric mode such as Q_+, already introduced by Prassides and Schatz in a multimode model.[37]

In a mean-field approach, such a two-mode vibronic model should involve two order parameters such as $\langle Q_- \rangle$ and $\langle Q_+ \rangle$; by symmetry they can be, respectively, identified to the $\langle \sigma \rangle$ and $\langle \sigma^2 \rangle$ order parameters of the biquadratic S=3/2 Blume-Sivardière Hamiltonian.[38,39]

Due to the huge dimension of the vibronic matrices associated with a two-mode two-orbital model, we have transformed the problem into a one-order parameter (i.e., one-mode) problem, by taking a ligand-field contribution proportional to the order parameter $\langle Q_- \rangle$, $\delta = \delta_0 + \alpha \langle |Q_-| \rangle$. The absolute value has been taken in order to respect the crystal-field invariance upon interchange of the molecular moities, i.e., the symmetry of Q_+. The model finally includes two intermolecular coupling parameters, η (cooperative localization parameter) and α (cooperative ligand-field parameter), but only one order parameter $\langle Q_- \rangle$ associated with the electronic localization.

III. VIBRONIC MODEL AND COMPUTATION

The two-orbital cooperative vibronic Hamiltonian already presented in Refs. 24, 25 is reexpressed here in shorter form, using matrix operators $\sigma^z, \sigma^x, \sigma^c$:

$$\hat{\sigma}^z = \begin{pmatrix} -1 & 0 & 0 & 0 \\ 0 & 1 & 0 & 0 \\ 0 & 0 & -1 & 0 \\ 0 & 0 & 0 & 1 \end{pmatrix}, \quad \hat{\sigma}^x = \begin{pmatrix} 0 & 1 & 0 & 0 \\ 1 & 0 & 0 & 0 \\ 0 & 0 & 0 & 1 \\ 0 & 0 & 1 & 0 \end{pmatrix},$$

$$\hat{\sigma}^c = \begin{pmatrix} 1 & 0 & 0 & 0 \\ 0 & 1 & 0 & 0 \\ 0 & 0 & -1 & 0 \\ 0 & 0 & 0 & -1 \end{pmatrix}$$

in the electronic basis $\psi_A^1, \psi_B^1, \psi_A^2, \psi_B^2$, where the subscripts A, B denote the molecular sites where the electron can be trapped, and superscripts 1,2 refer to the possible two orbitals.

The vibronic Hamiltonian, describing the system of coupled molecules, is written as

$$\hat{H} = \sum_i \left(\frac{\hat{P}_i^2}{2M} + \frac{1}{2} K \hat{Q}_i^2 \right) + \sum_i \not{\ell} \hat{Q}_i \hat{\sigma}_i^z + \sum_i J \hat{\sigma}_i^x + \sum_i \delta_0 \hat{\sigma}_i^c + \sum_{\langle i,j \rangle} \eta \hat{\sigma}_i^z \hat{Q}_j + \sum_{\langle i,j \rangle} \alpha \hat{\sigma}_i^c |\hat{Q}_j|$$

where $\hat{Q}_i$ is the nuclear operator associated with the asymmetric distortion mode Q_- of molecule i.

In this Hamiltonian, intra- and intermolecular terms are easily recognized:

(i) harmonic oscillators of mass M and stiffness K;

(ii) intramolecular vibronic coupling: $\not{\ell} \hat{Q}_i \hat{\sigma}_i^z$, favoring electronic localization;

(iii) transfer integral: $J \hat{\sigma}_i^x$, acting as a transverse field, favoring electronic delocalization;

(iv) intramolecular ligand field $\delta_0 \hat{\sigma}_i^c$, which basically monitors the competition between orbitals;

(v) $\eta \hat{\sigma}_i^z \hat{Q}_j$ is an intermolecular vibronic coupling term, between the electronic state of molecule i and the vibrational state of molecule j; it breaks the symmetry between the two

TABLE I. Computed parameters relative to the well-isolated orbitals (after Refs. 21, 23), η^c is the threshold value for the onset of low-temperature ordering. $T_{\mathrm{OD}}^{(1),(2)}$ are calculated with $\eta=0.42$, 0.75 (eV/Å), respectively.

HOMO	$\mathscr{l}$ (eV/Å)	J(cm^{-1})	η^c (eV/Å)	$\langle Q_- \rangle_{\mathrm{sat}}$ (Å)	$T_{\mathrm{OD}}^{(1),(2)}$ (K)
d_{xy}	1.79	10	$\ll 0.01$	0.06	280, 480
$d_{x^2-y^2}$	1.68	500	0.44	0.04	–,260

molecular sites; it acts as an electric field ($\sim W_d$ in the genuine PKS model) created by the electron trapping in the molecule j.

(vi) the last term is a cooperative crystal field which adds to the ligand-field term δ_0 and reinforces the competition between the two orbitals.

It must be recalled that we deal here with a particular case (molecular mirror symmetry), which leaves uncoupled the subspaces associated with the two orbitals.[24] We found it possible to treat the present Hamiltonian in the mean-field approach only. The summations over the distortion operators of the z neighbors are then replaced by mean-field parameters. The mean-field Hamiltonian is written as

$$\hat{H}_0=\frac{\hat{P}^2}{2M}+\frac{1}{2}K\hat{Q}^2+J\hat{\sigma}^x+(\mathscr{l}\hat{Q}+\eta\langle\hat{Q}\rangle_0)\hat{\sigma}^z+(\delta_0+\alpha\langle|\hat{Q}|\rangle_0)\hat{\sigma}^c,$$

where η and α stand for $z\eta_{ij}$ and $z\alpha_{ij}$. The matrix elements are given in the Appendix.

The resolution of the problem by minimizing the free energy cannot be obtained analytically, since it implies a nondiagonal 28×28 vibronic matrix. Alternatively, we obtained the self-consistent formulation of the problem by calculating the average value of the distortion operator, $\langle\hat{Q}\rangle_0$ in the eigenbasis of the mean-field Hamiltonian $\hat{H}_0$ (with which are associated the density operator $\hat{\rho}_0$ and the partition function Z_0):

$$\langle\hat{Q}\rangle_0=\mathrm{tr}(\hat{\rho}_0\hat{Q}).$$

The free energy per molecule is given by

$$F\leqslant -k_BT\ \ln(Z_0)+\langle\hat{H}-\hat{H}_0\rangle_0.$$

The second contribution of the free energy is the mean-field correction; it is easily written in terms of the thermal averages $\langle\hat{\sigma}^z\rangle_0,\langle\hat{\sigma}^c\rangle_0$, whose expressions, in turn, are determined from the eigenfunction coefficients:

$$\langle\hat{H}-\hat{H}_0\rangle_0=-\frac{1}{2}(\eta\langle\hat{\sigma}^z\rangle_0+\alpha\langle\hat{\sigma}^c\rangle_0)\langle\hat{Q}\rangle_0.$$

Computations are performed on a basis of dimension 4(electronic)$\times$7(vibrational). The truncature to the lowest seven vibrational states enables covering the pertinent energy range of the problem (see Ref. 21).

IV. RESULTS AND DISCUSSION

The present investigation is organized into three parts:

(i) double reentrance; (ii) first-order ferro-para transitions; (ii) double transitions.

Double reentrance can be obtained with a constant ligand-field parameter; we also briefly consider a variable ligand field: the study is carried out as a function of δ_0.

On the contrary, first-order and double transitions result from an orbital crossover which requires a thermal competition enhanced by a cooperative ligand field ($\alpha\neq0$): the corresponding studies are carried out as a function of δ_0 and α. The parameter values we use here are those determined for the biferrocenium cation,[13] and are listed in Table I.

We mainly focused on a cooperative localization parameter value $\eta=0.42$ eV/Å, common for both orbitals, which is just below the threshold value needed for the bad localizer to yield an ordered phase (see Table I). In such a case, the thermodynamic competition implies a low-temperature disordered phase (QMP) and, as a function of temperature, a paraelectric (PE) or a ferroelectric (FE) phase.

In addition, we considered a larger value of the cooperative localization parameter providing a thermodynamic competition between two ordered states, characterized by sizeably different values of the saturation distortion.

In Ref. 24 we presented stable or metastable solutions of the problem (as they emerged from the iterative resolution of self-consistent equation). Here we determine all the solutions, and we calculate their free-energy values. This enables

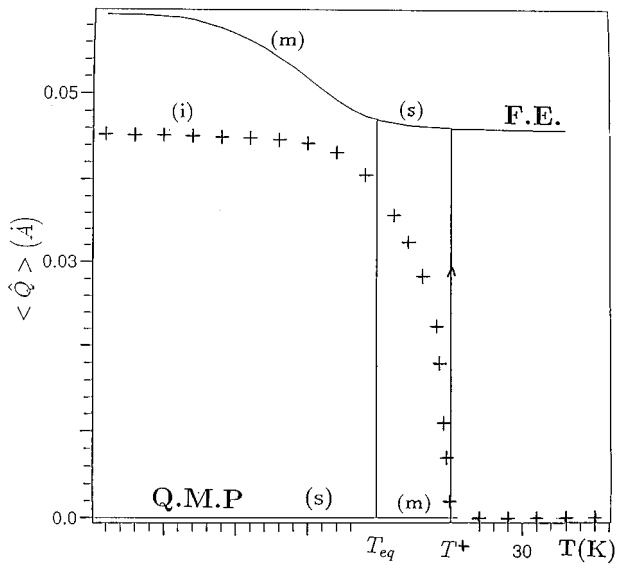

FIG. 3. Expanded view of curve 2, of Fig. 2. The stable, metastable, unstable characters of the states are denoted (s), (m), (i) respectively.

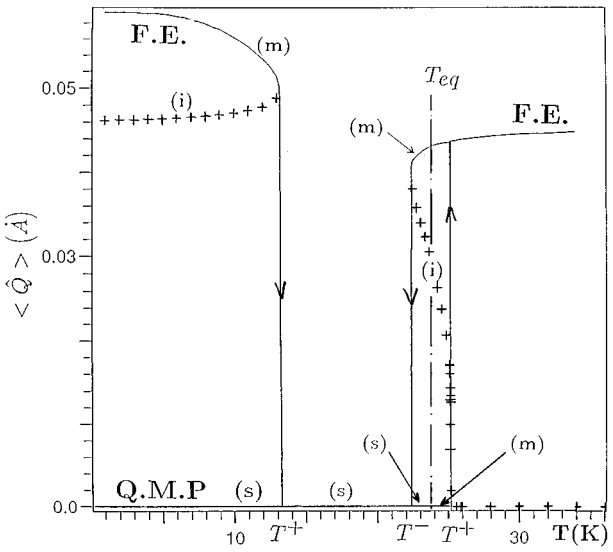

FIG. 4. Expanded view of curve 3 of Fig. 2. Note the metastable character of the low-temperature FE phase (''second reentrant'').

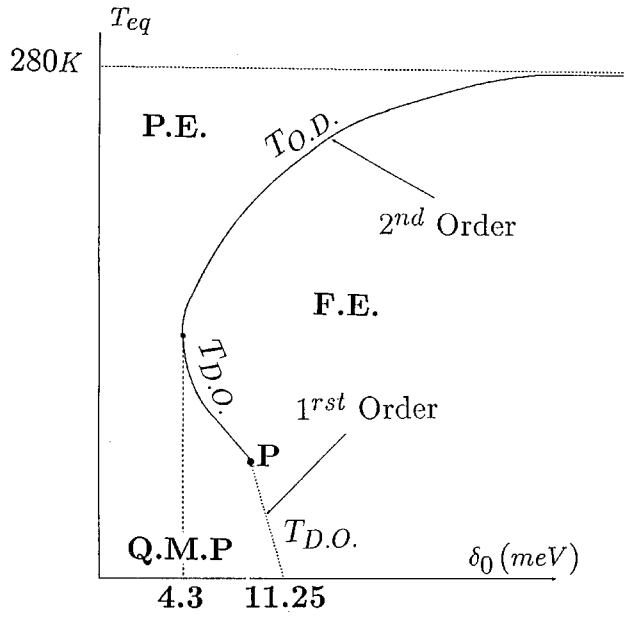

FIG. 5. Schematic phase diagram of the system. Second-order and first-order branches meet at a tricritical point **P**.

us to determine thermal hysteresis loops. We stress their open/closed character, since a closed character of the loop is needed for reversible information storage.

For clarity, the phase diagrams representing the transition temperatures versus static field δ_0 or cooperative ligand-field parameter α are systematically reported. Due to the variety of the thermal behaviors, the equilibrium transition temperatures may be order-disorder, disorder-order, order-order (on increasing temperatures), and will be reported as T_{OD}, T_{DO}, T_{OO}, respectively.

A. Double reentrance

We follow here the thermodynamic competition, as function of a constant ligand field δ_0, between the QMP and the ordered phase.

We show in Fig. 2 the successive order-parameter/ temperature diagrams for different values of δ_0. The thermal behavior of the system is closely related to the stable, metastable or unstable character of the various solutions. The prominent feature of the diagram is the crossing of two branches, for a critical value of the ligand field $\delta^* = 11.08$ meV here.

On decreasing δ_0 from large positive values, the system displays five typical situations, corresponding to the five different curves of Fig. 2:

(i) $\delta_0 \gg \delta^*$, the good localizer orbital is involved alone. The order-parameter / temperature diagram displays a single nontrivial branch, corresponding to a FE stable state. The FE/PE order-disorder transition is of second order. The system behaves as a simple mean-field Ising system (actually, an Ising model with a negligible transverse field). For moderate values of δ_0, the thermal population of the low-energy bad-localizer orbital induces a sizable distortion of the low-temperature part of curve (1).

(ii) 11.08 meV $= \delta^* < \delta_0 < \delta^{(1)} = 11.30$ meV. The diagram (Fig. 2, curves 2) displays, at low temperature, a third solution. These curves are better visualized on a larger scale in Fig. 3. The third solution is unstable, and its limiting temperature, denoted T^+, can be described as the upper temperature of an open hysteresis loop.

The QMP phase state, involving the bad localizer orbital, is stable at zero temperature for $\delta_0 < \delta^{(2)} = 11.25$ meV. This actually is the case reported in Fig. 3, where an equilibrium temperature T_{eq} appears. It is worth noting that the QMP state cannot be reached by thermal continuity (i.e., by varying temperature alone), because of the open character of the hysteresis loop. This situation ceases for $\delta_0 = \delta^*$.

(iii) For 10.50 meV $= \delta_{(3)} < \delta_0 < \delta^* = 11.08$ meV, the diagram is drastically modified (Fig. 2 curves 3, shown on a larger scale in Fig. 4). The reentrant QMP phase, mainly due to the bad localizer orbital, is stable and can be reached by

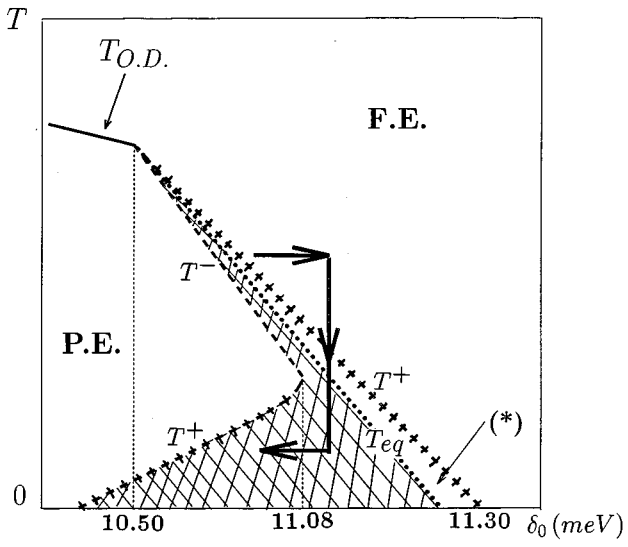

FIG. 6. Diagram of the metastable phases: Hatched area: metastable FE / stable QMP, starred (*) area: stable FE/metastable QMP. The arrows schematize a pathway for trapping the metastable FE state.

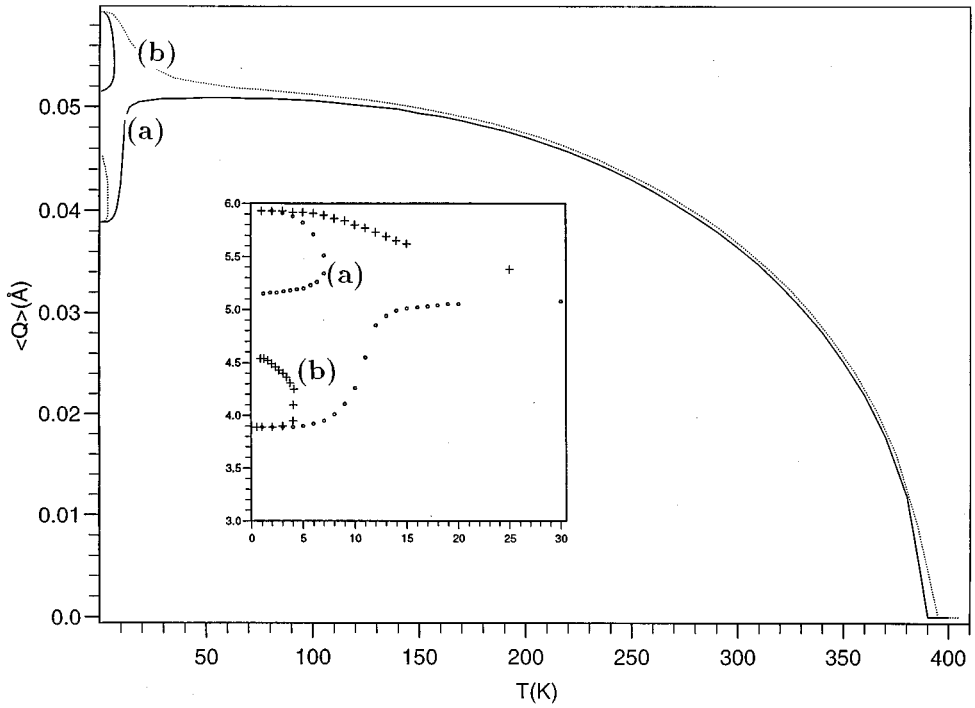

FIG. 7. Thermal dependence of the order parameter, in the case of a large intermolecular coupling parameter: $\eta = 0.75$ eV/Å, $\delta_0 =$ (a) 8.5 meV, (b) 8.0 meV.

thermal continuity. The low-temperature FE phase, here denoted ''*second reentrant,*'' is metastable. We indicate that such a metastable character is also obtained when using, alternatively, an elastic intermolecular coupling term ($\eta \hat{Q}_i \hat{Q}_j$ as presented in Ref. 40).

(iv) For 4.3 meV $= \delta^{(4)} < \delta_0 < \delta^{(3)} = 10.50$ meV, the diagram comprises a single branch (Fig. 2 curve 4). When the limiting two transitions of the FE phase are both second order, it is observed that the ground vibronic state, at all temperatures, is based on the bad localizer orbital. Then the FE state originates from excited states, based on the good localizer orbital. As already noticed in Ref. 25, the eventual first-order character of the low-temperature transition is associated with a simultaneous crossover of the vibronic ground state. The reentrant QMP state, obviously, is reachable by thermal continuity.

(v) For $\delta_0 < 0.006$ meV, the diagram only contains the trivial, PE state (curve 5). The vibronic states based on the good localizer orbital are too high in energy to have any influence.

We show in Fig. 5 the computed variation of the equilibrium temperatures as a function of the ligand-field parameter δ_0. This actually is the *equilibrium* phase diagram of the system.

Using the data of the hysteresis loops, we have drawn in Fig. 6, the diagram of the metastable phases. The particular shape of the FE metastable phase (hatched area) is responsible for the second reentrance.

From the point of view of information storage, the second reentrant state cannot be reached by a purely thermal addressing. According to the phase diagram reported in Fig. 6, more complex pathways are needed, involving a variation of the ligand-field term. This might be achieved using an applied stress or an external pressure. A possible pathway is schematized in Fig. 6: the system is cooled down under stress, and the metastable FE state is trapped when stresses are released.

Using the larger value of the intermolecular coupling parameter ($\eta = 0.75$ eV/Å), similar phenomena are obtained; they now involve strongly and weakly polarized states, for which typical plots are reported in Fig. 7.

B. First-order ferro-paraelectric transitions

In this subsection, we consider a thermodynamic competition enhanced by a cooperative ligand field ($\alpha \neq 0$) of adequate sign and magnitude, so as to yield a good-to-bad localizer orbital crossover, from an ordered to a disordered state. It is convenient to establish the relationships between α, δ_0, η, which are needed for obtaining such a crossover. As a first approach, by only considering the lowest two vibronic states of each orbital, a four-state scheme, analogous to the Blume-Sivardière Hamiltonian, is obtained. This is shown in Fig. 8, which makes clear two requirements:

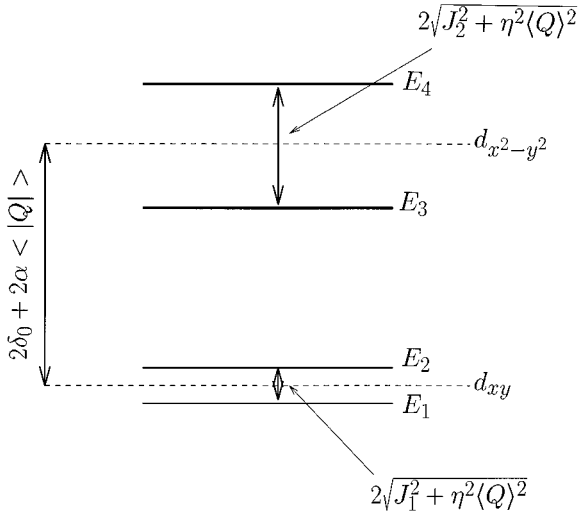

FIG. 8. Truncated representation of the vibronic energy scheme.

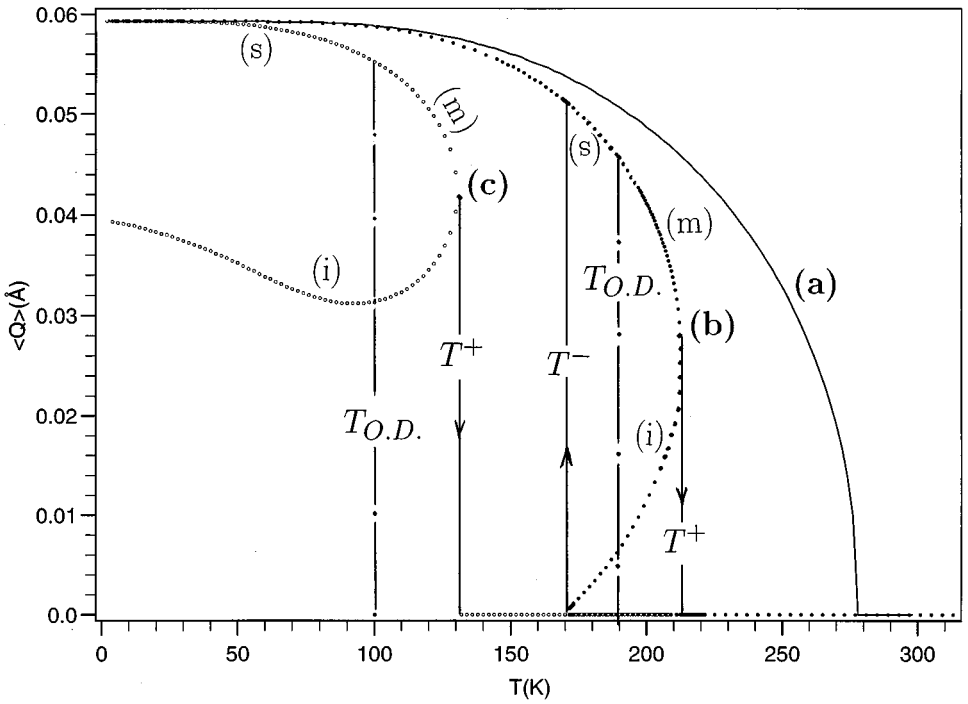

FIG. 9. Thermal variation of the order parameter computed for $\alpha=\eta=0.42$ eV/Å, $\delta_0=(a)50$ meV, (b) 8 meV, and (c) -5 meV. The stable, unstable, metastable characters of the solutions are labeled (s), (i), (m), respectively.

(i) the good localizer orbital must become the ground state at low temperature, in the ordered state,

(ii) the bad localizer orbital, must become a rather well isolated ground state, in the high-temperature disordered state.

Analytically:

(i) at $T=0$: $E_3-E_1>0\Rightarrow 2\delta_0-J_2>-(\eta+2\alpha)\langle Q\rangle_0$, where $\langle Q\rangle_0$ is the value at $T=0$ K of the distortion created by the good localizer orbital; practically it is a constant of the problem, $\langle Q\rangle_0=0.06$ Å.[30,31]

(ii) at $T>T_{eq}$: $E_3\ll E_1=0\Rightarrow\ \delta_0\ll(J_2-J_1)/2\simeq 31.5$ meV.

To summarize, first-order transitions may be obtained for a limited range of ligand-field values:

$$\delta_0^{\min}<\delta_0<\delta_0^{\max}$$

with

$$\delta_0^{\min}=\frac{1}{2}[J_2-(\eta+2\alpha)\langle Q\rangle_0],$$

$$\delta_0^{\max}\ll\frac{1}{2}(J_2-J_1)\quad(\text{assuming } J_2>J_1).$$

Both $\delta_0^{\min}$ and $\delta_0^{\max}$ are functions of the parameters α, η, so that the phase diagram of the system is expected to be quite intricate. We report here a few partial views of this phase diagram.

1. Dependence upon δ_0

We fixed the coupling parameter values: $\eta=\alpha=0.42$ eV/Å.

The investigated range of ligand-field values was -50 meV$\leqslant\delta_0\leqslant+50$ meV. The results plotted in the Figs. 9 and 10, show that

(i) first order transitions [curves (b), (c) in Fig. 9] are obtained for $\delta_0^{\min}\simeq-10$ meV$\leqslant\delta_0\leqslant\delta_0^{\max}\simeq 26$ meV, in agreement with the preliminary analysis reported above. *P* associated to $\delta_0^{\max}$ in Fig. 10, is the tricritical point of the phase diagram;

(ii) The thermal hysteresis loops, defined by the limiting temperatues T^-, T^+, are closed for 4.3 meV$\leqslant\delta_0\leqslant\delta_0^{\max}$; reversible thermal addressing of information storage is possible;

(iii) for lower δ_0 values, the hysteresis loops are *open*; this results from the occurence at $T=0$ K of a QMP phase (firstly metastable, then stable on decreasing δ_0). In other terms, T^- is negative [curve (c) in Fig. 9].

In case (c), the low-temperature FE phase cannot be reached by thermal continuity: thermal addressing of information storage is no longer possible.

2. Dependence upon α

Keeping $\eta=0.42$ eV/Å, the ligand-field value $\delta_0=15$ meV was taken in the middle of the range studied in the

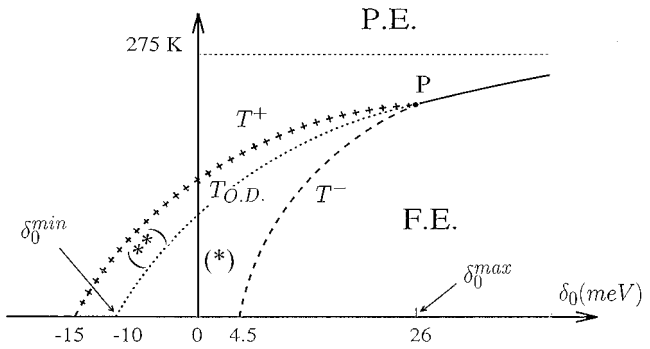

FIG. 10. Phase diagram in axes (T, δ_0), for $\alpha=\eta=0.42$ eV/Å. Second- (first-) order transitions are represented by full (broken) lines. The areas denoted (*), (**), respectively, correspond to stable FE/metastable PE and the reverse.

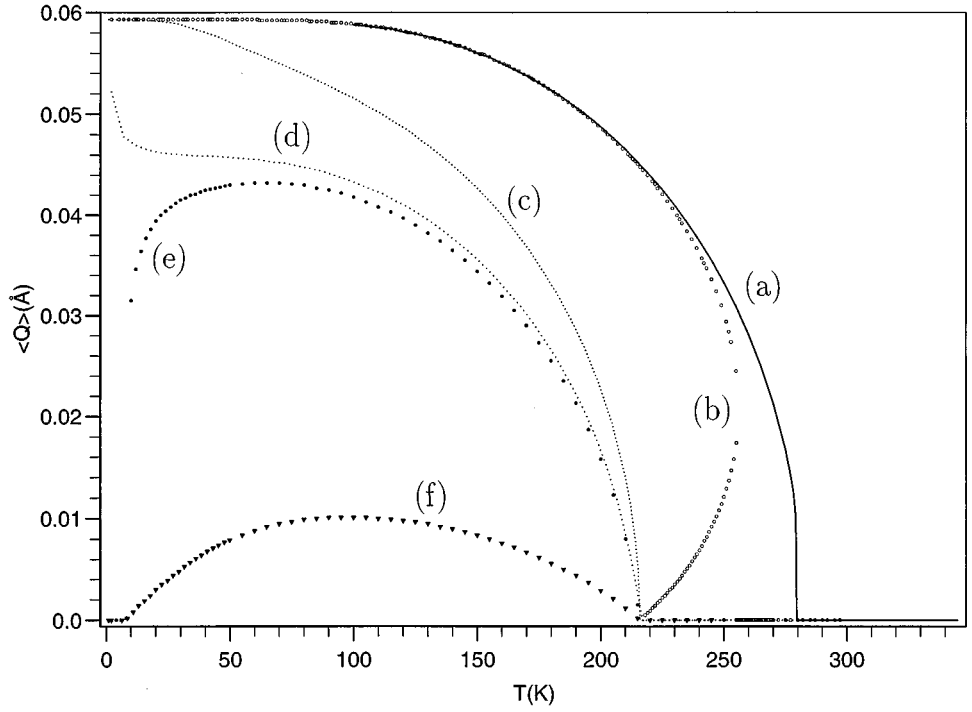

FIG. 11. Thermal variation of the order parameter computed for $\delta_0 = 15$ meV, $\eta = 0.42$ eV/Å, and $\alpha = 6,1,0,-0.085,-0.1,-1$ eV/Å from (a) to (f), respectively.

previous section. For $\alpha = 0$, at all temperatures, the ground state is based on the good localizer orbital, a second-order transition is obtained, but low-lying excited states based on the bad localizer orbital will interfer, either at high or low temperature, when the thermodynamic competition is enhanced by $\alpha > 0$ or < 0, respectively:

(i) $\alpha > 0$. (Figs. 11(a) and 11(b)]. Above the threshold value 0.8 eV/Å, the order-disorder transition is first order; at 4.5 eV/Å, it is second order again. This is due to the α dependence of $\delta_0^{\min}$, $\delta_0^{\max}$. The phase diagram exhibits two tricritical points (P_1, P_2 in Fig. 12).

(ii) $\alpha < 0$ [Fig. 11(d)–11(f)]. Below the threshold value $\simeq -0.1$ eV/Å, the bad localizer is the low-temperature ground state. Reentrant phases are observed, with properties similar to those previously studied (progressive or abrupt bad-to-good orbital crossover); a third tricritical point is obtained (P_3 in Fig. 12).

A similar study has been performed with the larger value of the intermolecular interaction parameter, $\eta = 0.75$ eV/Å. The phase diagram, plotted in Fig. 13, exhibits two critical points, but no longer (of course) the QMP phase. Closed or open hysteresis loops may be obtained as well.

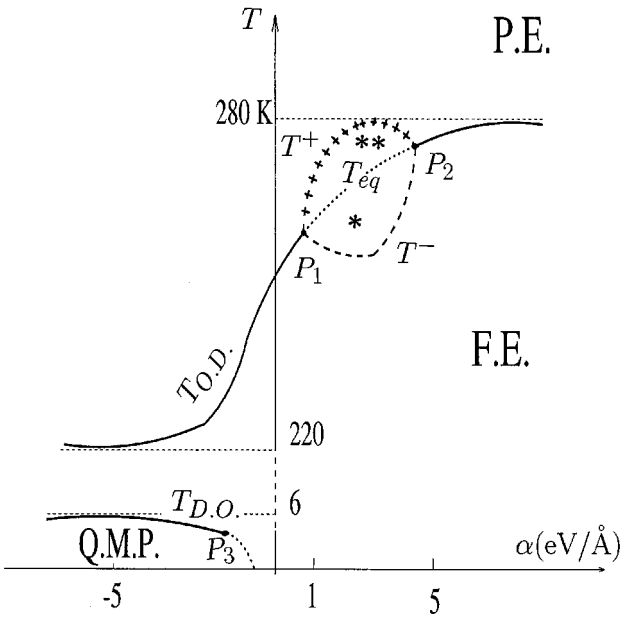

FIG. 12. Phase diagram in axes (T, α) for $\delta_0 = 15$ meV.

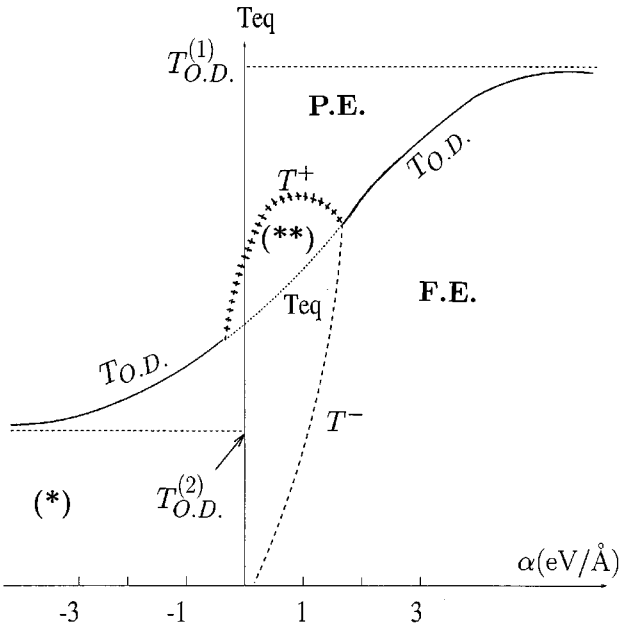

FIG. 13. Phase diagram in axes (T, α) for $\delta_0 = 15$ meV and $\eta = 0.75$ eV/Å. Note the open character of the hysteresis loop for $\alpha < 0.2$ eV/Å.

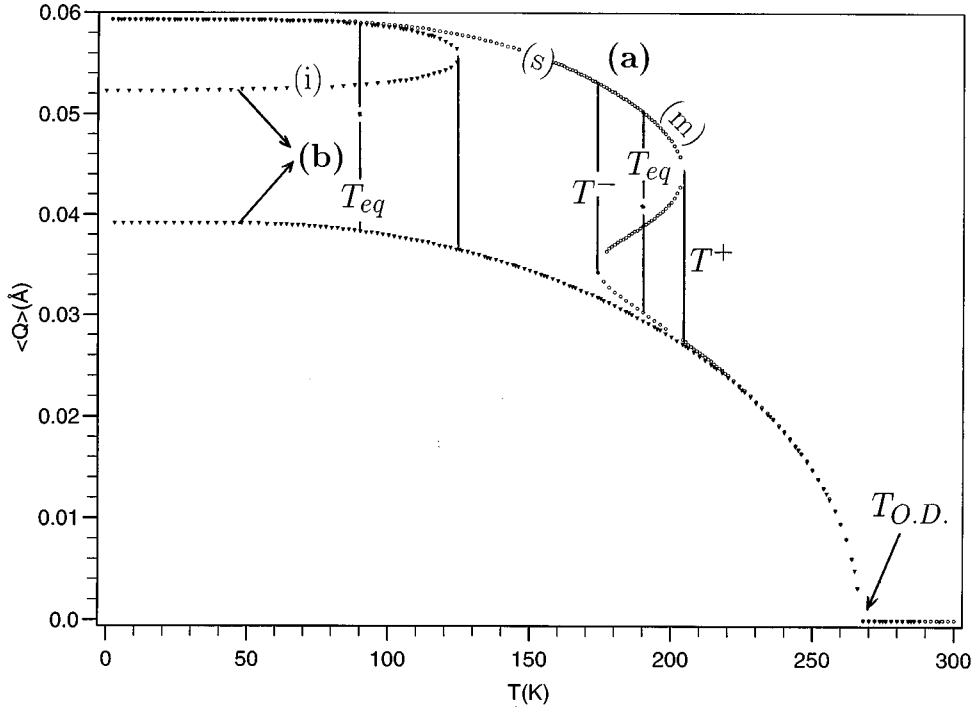

FIG. 14. Thermal variation of the order parameter, computed for $\alpha=3$ eV/Å, $\eta^{(1)}=0.76$ eV/Å, $\eta^{(2)}=0.42$ eV/Å, and $\delta_0=$(a)-100 meV, (b)-120 meV.

C. Double transitions

Double transitions (order-order + order-disorder transitions, on increasing temperature) result from the thermal competition between ordered states corresponding to the two orbitals. To start with, we focus on good-to-bad localizer orbital crossovers. We easily found such double transitions in a particular case, where η_1, η_2 have been tuned so as to provide an identical order-disorder temperature for both orbitals: $\eta_1=0.76$ eV/Å, $\eta_2=0.4$ eV/Å, $T_{\mathrm{OD}}^{(1)}=T_{\mathrm{OD}}^{(2)}=270$ K.

Such crossovers are shown in Figs. 14(a) and 14(b) obtained with $\alpha=3$ eV/Å, $\delta_0=-100,-120$ meV, respectively.

The phase diagram as a function of δ_0, for $\alpha=3$ eV/Å, is shown in Fig. 15. The ending point **S** of the three branches corresponds to the collapse of the hysteresis loop; this occurs at temperatures lower than the order-disorder temperature (T_{OD}): the order-disorder and order-order transitions are disconnected. For smaller α values, the order-order temperature shifts towards the order-disorder temperature; the ending point *S* moves towards the tricritical point *P* of Fig. 10.

In principle, similar crossovers may be expected as well from bad-to-good localizer orbital. As a matter of fact, we did not find them; this may be just a matter of numerical values, since we succeeded when we used a similar model with interaction written in elastic form $\eta\hat{Q}_i\hat{Q}_j$.

Smooth effects, due to the thermal population of excited levels, can be also obtained, leading to s-shaped distortions of the low-temperature part of the $\langle Q_-(T)\rangle$ curve;[24] good-to-bad and bad-to-good progressive crossovers have been obtained as well.

V. DISCUSSION

It clearly appears that the phase diagram of the system, with respect to the whole parameter set of the problem, is extremely complicated; it is not discussed here. We focus here on the *thermal bistability* associated with the abrupt transitions—with hysteresis—due to the orbital crossovers.

Such a bistability fulfills all criteria of the ''molecular bistability'' previously defined by Kahn and Launay.[1] Of major interest are the optical properties, which strongly differ from one state to the other, and should allow optical reading of information. An unanswered question is the relaxation rate between these states (a preliminary investigation is briefly reported in Ref. 41). In terms of the applicability of mixed-valence solids to information, storage, an interesting problem arises from the presence of open thermal hysteresis loops, which prevents information from being thermally addressed. We shall investigate in a future work, the alternative way of electric addressing, taking advantage of the double

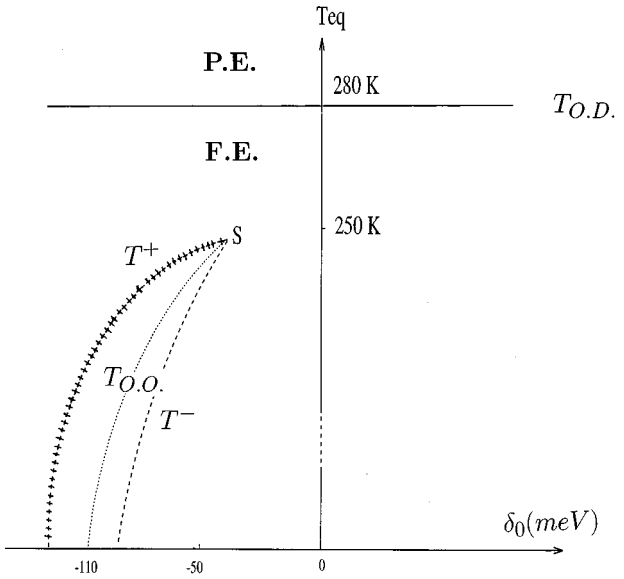

FIG. 15. Phase diagram in axes (T, δ_0), associated with Fig. 14.

bistability (quantum mechanical and thermal) of the system. It is worth noting that the presence of open hysteresis loops has not been reported so far in the case of the spin-transition solids, although it should occur by combining low transition temperature and large cooperativity.

We briefly discuss the applicability of the present results to a wider class of materials. Basically, the existence of bistability needs a combination of the following features:

(i) Electric polarizability; here mixed-valence systems provide a large polarizability; induced electric dipole moments are large (electron charge x metal-metal distance); ionocovalent solids including heavy atoms should certainly possess an interesting polarizability and, as a matter of fact, some of them exhibit a ferro-paraelectric transition;

(ii) An ambiguous response of the system to external perturbations; in the present case, this is due to the quasidegeneracy of the HOMO of the moities; more generally, for molecular solids, it may originate from a quasi-Jahn-Teller instability associated with a centrosymmetric distortion mode (which does not create electric polarization); for ionocovalent solids, the problem might be put in terms of nonlinear polarizability, by analogy to optical bistability;[9,10] as a matter of fact a textbook example of reentrant PE phase is Seignette's salt.

(iii) Cooperativity, for both electric polarization (through dipole fields) and molecular bistability; in molecular solids, we put the latter in terms of a cooperative crystal field; more generally speaking, mechanisms leading to solid-state transitions (metal-insulator, Peierls instability . . .) are possibly relevant.

VI. CONCLUSION

The thermodynamic properties associated with the two-orbital cooperative vibronic (PKS) model have been reported in terms of a molecular bistability, involving both a cooperative localization and a cooperative ligand field responsible for orbital crossovers.

We focused on the consequences of cooperative orbital crossovers: first-order para-ferroelectric, and ferro-ferroelectric transitions have been characterized, and their thermal hysteresis loops determined. We found, in some cases, an open hysteresis loop which prevents information storage from being thermally addressed with a reversible effect.

The open question of the stability of the second-reentrant phase has been answered in the frame of the present vibronic theory. Similar investigations in other models yielding double reentrance are of interest.

ACKNOWLEDGMENTS

Laboratorie de Magnetisme et d'Optique is supported by CNRS (URA No. 1531).

APPENDIX

Mean-field Hamiltonian matrix elements in the one-mode two-orbital model:

$$\langle \Phi^{\pm}_{1,n}|\hat{H}_0|\Phi^{\pm}_{1,n}\rangle = \left(n+\frac{1}{2}\right)h\nu_- - \delta_0 - \alpha\langle|\hat{Q}|\rangle_0 \pm J_1,$$

$$\langle \Phi^{\pm}_{2,n}|\hat{H}_0|\Phi^{\pm}_{2,n}\rangle = \left(n+\frac{1}{2}\right)h\nu_- - \delta_0 - \alpha\langle|\hat{Q}|\rangle_0 \pm J_2,$$

$$\langle \Phi^{\pm}_{1,n}|\hat{H}_0|\Phi^{\mp}_{1,n+1}\rangle = \frac{-\ell_1}{\sqrt{2}}\sqrt{\frac{h\nu_-}{K}}\sqrt{n+1},$$

$$\langle \Phi^{\pm}_{2,n}|\hat{H}_0|\Phi^{\mp}_{2,n+1}\rangle = \frac{-\ell_2}{\sqrt{2}}\sqrt{\frac{h\nu_-}{K}}\sqrt{n+1},$$

$$\langle \Phi^{\pm}_{1,n}|\hat{H}_0|\Phi^{\mp}_{1,n}\rangle = \eta_1\langle\hat{Q}\rangle_0,$$

$$\langle \Phi^{\pm}_{2,n}|\hat{H}_0|\Phi^{\mp}_{2,n}\rangle = \eta_2\langle\hat{Q}\rangle_0,$$

where $\Phi^{\pm}_{i,n} = (1/\sqrt{2})[\psi^i_A(\vec{r}) \pm \psi^i_B(\vec{r})]\chi_n(Q_-)$ [$(i=1, 2)$, with $\chi_n(Q_-)$ the nth eigenfunction of the harmonic oscillator (note the electronic and vibronic nondiagonal terms].

The spin 3/2 Hamiltonian

In parallel to the present vibronic calculations, we undertook the thermodynamical investigation of the spin-3/2 Hamiltonian already studied by Blume.[20] In the present case, the $\pm 3/2$ states of the fictitious spin represent the lowest two vibronic states of the good localizer orbital, while $\pm 1/2$, are those of a bad localizer. We introduce between these states transverse field terms representing the electron transfer, as well as pair contributions associated with all intermolecular terms of the vibronic Hamiltonian. With this complete form, the spin $S=3/2$ Hamiltonian has not been investigated so far.

The most important results of the vibronic model are provided by the present $S=3/2$ Hamiltonian, solved in the mean-field approach, and are revealed to be a qualitative truncature of the correct vibronic problem. Clearly, some of the results associated with the case of both polarizable orbitals (for instance the double transitions shown in Figs. 7 and 14) could not be reproduced by the $S=1$ Blume-Emery-Griffiths Hamiltonian, we used in a previous work.[9]

The $S=3/2$ Hamiltonian is written

$$\hat{H} = -\sum_{ij} J_{ij}\hat{\sigma}^z_i\hat{\sigma}^z_j - \sum_{ij} K_{ij}\left[(\hat{\sigma}^z_i)^2 - \frac{1}{3}S(S+1)\right](\hat{\sigma}^z_j)^2 - \sum_i \Delta_i\left[(\hat{\sigma}^z_i)^2 - \frac{1}{3}S(S+1)\right] + \sum_i \Omega_1\hat{\sigma}^x_{1,i} + \sum_i \Omega_2\hat{\sigma}^x_{2,i},$$

where the $\hat{\sigma}^z$ and the $\hat{\sigma}^x$ operators are

$$\hat{\sigma}^z = |3/2\rangle\langle 3/2| - |-3/2\rangle\langle -3/2| + |1/2\rangle\langle 1/2| - |-1/2\rangle\langle -1/2|,$$

$$\hat{\sigma}^x_1 = |3/2\rangle\langle -3/2| + |-3/2\rangle\langle +3/2|,$$

$$\hat{\sigma}^x_2 = |1/2\rangle\langle -1/2| + |-1/2\rangle\langle 1/2|.$$

J, J', respectively, couple the $\pm\frac{3}{2},\pm\frac{1}{2}$ states, and compares to the vibronic energy term $\eta\langle\hat{Q}\rangle$; Δ and K are the static ''anisotropy'' terms, respectively intra- and intermolecular; Ω_1,Ω_2 are the tunneling matrix elements, associated with the two orbitals.

The $S=3/2$ Hamiltonian involves two order parameters $m=\langle\hat{\sigma}^z\rangle$, $q=\langle(\hat{\sigma}^z)^2\rangle$. m is associated with the symmetry breaking (i.e., electric polarization) of the molecules; q is associated with the (thermal) relative populations of the competing orbitals.

The mean-field free energy of the four-state Hamiltonian is

$$F_{\mathrm{mf}}=\frac{3}{4}Jm^2+\frac{1}{4}Kq^2-k_BT\ln(Z).$$

The partition function Z is deduced

$$Z=2e^{-\beta(\Delta-Kq^2)}\cosh\beta\sqrt{\frac{9}{4}J^2m^2+\Omega_1^2}$$

$$+2e^{\beta(\Delta-Kq^2)}\cosh\beta\sqrt{\frac{1}{4}J^2m^2+\Omega_2^2}.$$

The coupled self-consistent equations leading to the $m(T)$, $q(T)$ set of the values are provided by

$$\frac{\partial F_{\mathrm{mf}}}{\partial m}=0 \quad\text{and}\quad \frac{\partial F_{\mathrm{mf}}}{\partial q}=0.$$

[1] O. Kahn and J.P. Launay, Chemtronics **3**, 140 (1989).
[2] C. Joachim and J.P. Launay, Chem. Phys. **109**, 93 (1986).
[3] S. Woitellier, J.P. Launay, and C. Joachim, Chem. Phys. **131**, 481 (1989).
[4] J. Zarembovitch and O. Kahn, New. J. Chem. **15**, 1811 (1991).
[5] J.H. Ammeter, Nouv. J. Chim. **4**, 631 (1980).
[6] E. König, Struc. Bonding (Berlin) **76**, 51 (1991).
[7] P. Gütlich and A. Hauser, Coord. Chem. Rev. **97**, 21 (1990).
[8] P. Gütlich, A. Hauser, and H. Spiering, Angew. Chem. Int. Ed. Engl. **33**, 2024 (1994).
[9] J. Zarembovitch, Mol. Cryst. Liq. Cryst. **234**, 243 (1993).
[10] C. Roux, J. Zarembovitch, B. Gallois, T. Granier, and R. Claude, Inorg. Chem. **33**, 2273 (1994).
[11] M.B. Robin and P. Day, Adv. Inorg. Chem. Radiat. Chem. **10**, 247 (1967).
[12] N. Hush, Prog. Inorg. Chem. **8**, 357 (1967).
[13] D.N. Hendrickson, in *Mixed Valence Systems: Applications in Chemistry, Physics, and Biology*, Vol. 343 of *NATO Advanced Studies Institute, Series B: Physics*, edited by K. Prassides (Kluwer, Dordrecht, 1991), pp. 67–90.
[14] M. Sorai, A. Nishimori, D.N. Hendrickson, T.Y. Dong, and M.J. Cohn, J. Am. Chem. Soc. **109**, 4266 (1987).
[15] T. Kambara, D.N. Hendrickson, T.Y. Dong, and M.J. Cohn, J. Chem. Phys. **86**, 2362 (1987).
[16] T. Kambara and N. Sasaki, J. Coord. Chem. **18**, 129 (1988).
[17] M. Blume, V.I. Emery, and R.B. Griffiths, Phys. Rev. A **4**, 1071 (1971).
[18] K. Boukheddaden, J. Linares, S. Galam, and F. Varret, J. Phys. **5**, 469 (1993); **5**, 5179 (1993).
[19] S.B. Piepho, E.R. Krausz, and P.N. Schatz, J. Am. Chem. Soc. **100**, 2996 (1978).
[20] P.N. Schatz, in *Mixed Valence Systems: Applications in Chemistry, Physics, and Biology* (Ref. 13), pp. 7–28.
[21] K. Boukheddaden, J. Linares, A. Bousseksou, J. Nasser, H. Rabah, and F. Varret, Chem. Phys. **170**, 147 (1993).
[22] K. Boukheddaden, J. Linares, and F. Varret, Chem. Phys. **172**, 239 (1993).
[23] K. Boukheddaden, J. Linares, and F. Varret, Phys. Rev. B. **47**, 14 070 (1993).
[24] J. Linares, K. Boukheddaden, and F. Varret, Chem. Phys. **182**, 225 (1994).
[25] K. Boukheddaden, J. Linares, and F. Varret, Phys. Rev. B **49**, 15 659 (1994).
[26] S.I. Klokishner and B.S. Tsukerblat, Chem. Phys. **125**, 11 (1992).
[27] S.I. Klokishner, B.S. Tsukerblat, and B.L. Kushkuley, Phys. Lett. A **179**, 429 (1993).
[28] K. Kasono and I. Iono, Z. Phys. B **88**, 205 (1992); **88**, 213 (1992).
[29] C. Buzano and A. Pelizzola, Phys. A **189**, 337 (1992).
[30] D.O Cowan, P. Shu, E.L. Hedberg, M. Rossi, and T.J. Kistenmacher, J. Amer. Chem. Soc. **101**, 1304 (1979).
[31] H. Sano, Hyp. Inter. **53**, 97 (1990).
[32] K.A. Müller and H. Bukhard, Phys. Rev. B **19**, 1123 (1976).
[33] J.G. Bednorz and K.A. Müller, Phys. Rev. Lett. **52**, 2289 (1984).
[34] P.G. De Gennes, Solid State Commun. **1**, 132 (1963).
[35] R.B. Stinchcombe, J. Phys. C **6**, 2459 (1973).
[36] M. Nakano, M. Sorai, P.M. Hagen, and D.N. Hendrickson, Chem. Phys. Lett. **196**, 186 (1992).
[37] K. Prassides and P.N. Schatz, J. Phys. Chem. **93**, 83 (1989).
[38] F.C. SA Barreto and O.F. De Alcantara Bonfim, Physica A **172**, 378 (1991).
[39] J. Sivardière and M. Blume, Phys. Rev. B **5**, 1126 (1991).
[40] K. Boukheddaden, J. Linares, S. Galam, and F. Varret, Chem. Phys. **180**, 43 (1994).
[41] F. Varret, J. Linares, and K. Boukheddaden, Chem. Phys. (to be published).